LANGMUIR

pubs.acs.org/Langmuir Article

Slip Effects on Ionic Current of Viscoelectric Electroviscous Flows through Different Length Nanofluidic Channels

Tumcan Sen and Murat Barisik*

Cite This: *Langmuir* 2020, 36, 9191−9203 Read Online

ACCESS | Metrics & More | Article Recommendations

ABSTRACT: The pressure driven slip flow of an electrolyte solution is studied through different nanofluidic channel lengths at varying salt concentrations. The viscous-thickening due to the electrostatic interactions within the electric double layer and the reverse ionic transport due to the streaming potential are developed. The influence of the Navier slip boundary condition is described under both electroviscous and viscoelectric effects with a surface charge regulation (CR) model while the observed behavior is compared and validated with molecular dynamic (MD) calculations from multiple studies. Results show that electroviscous and viscoelectric effects decrease transport. Earlier studies at the no slip boundary presented an increase of ionic current by increasing salt concentration and decreasing channel length. In contrast, our study found that the ionic current occurred almost independent of both salt concentration and channel length, except for very short channels and very low salt concentrations, when electroviscous and viscoelectric effects were considered. In the case of the constant slip length condition, ionic conduction was enhanced, but velocity slip developing on surfaces showed significant variation based on the salt concentration and channel length. This is due to the natural CR behavior enhancing the surface charge and consequential near surface electrohydrodynamics as a result of increase in salt concentration and/or decrease of channel length. Considering that the electroviscous effect alone creates up to 70% lower velocity slips than Poiseuille flow predictions, while further including the viscoelectric effect, results in an almost no-slip condition at high salt concentrations and/or short channels. As a result, the ionic current of a viscoelectric electroviscous slip flow is found to be equal to 1/3 of an electroviscous slip flow and to decrease with a decrease in the channel length.

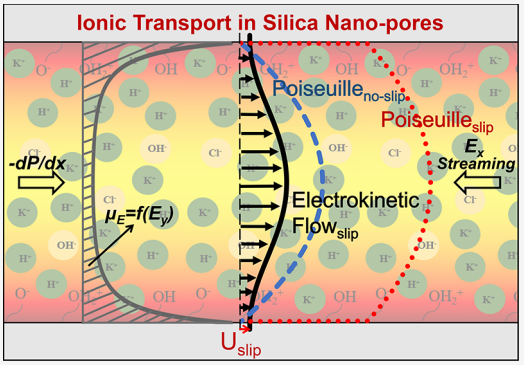

INTRODUCTION

Recent advances in nanotechnology have provided widespread usage of nanofluidic devices in various fields. This also presents new complications that need to be addressed. Yet, many promising applications such as sensing and filtration technologies,[1,2] water desalination,[3] ionic diodes/transistors,[4,5] energy storage/production,[6] artificial organs,[7] and e-ink technology[8] are all worth the additional effort. The fundamental principles behind these systems depends on the movement of charged species through an aqueous medium. Such ionic transport is determined by both fluid dynamics and electrokinetic interactions at nanoscale that liquid/solid momentum coupling at the interfaces and ionic layering over the surfaces plays a major role.[9−11] However, an accurate description of the ionic transport in nanoconfinements is still missing.

When a pressure gradient is applied across a nanofluidic channel, whose height is comparable to the electric double layer (EDL) thickness (λ), counterions within the EDL are carried along creating an "ionic/streaming current".[12] As a consequence, carried counterions accumulated in the downstream develop a potential bias across the channel resulting in a reverse ionic transport opposite to fluid flow[13] called "conduction current". There are many studies dedicated to understanding the ionic transport through nanofluidic systems. The majority of these theoretical analyses examined the attenuating effect of conduction current on flow rate by an apparent increase in the viscosity as "electroviscous effect",[14−21] which was found to reduce the ionic transport. Electroviscosity increases with an increased overlap of EDL from opposing surfaces that decrease salt concentration[14] and/or by decrease confinement height reducing the ionic current. Researchers employed the Debye−Hückel parameter (H/λ) to quantify electroviscosity effects.[16,22] Increase in surface zeta potential causes electroviscosity to increase[15] until the zeta potential reaches a threshold above which EDL becomes thin and electroviscosity becomes negligible.[15] In addition, the actual fluid viscosity eventually develops significant local

Received: May 18, 2020
Revised: July 7, 2020
Published: July 7, 2020

https://dx.doi.org/10.1021/acs.langmuir.0c01457
Langmuir 2020, 36, 9191−9203

thickening due to the electrostatic interactions within the EDL identified as the "viscoelectric effect".[23] There are only few researchers focused on viscoelectric effects on ionic current,[24,25] and they concluded that viscoelectric effects decrease the ionic current in a pressure driven flow. Researchers also focused on ionic diffusion effects in the axial direction, especially for short channels and pores. The diffusive interactions between the reservoir and channel alter the ionic condition and surface charge through the so-called "ionic development length" regions (as long as 2.7 times Debye length (λ)).[26,27] To resolve this channel−reservoir equilibrium in the axial direction, the most accurate and recent studies employed two-dimensional solution of coupled Poisson−Nernst−Planck (PNP) and Navier−Stokes (NS) equations.[28−30] The dependence of ionic current on the channel length is addressed in some studies that decreasing channel resistance by decreasing channel length was found to increase the ionic current.[31,32] In addition, studies also discussed the effects of concentration polarization at the channel entrance and exit regions[28,29,31] which develops access resistance and decreases the ionic current.[32] So far, there is no published work that combines the occurrence of these three major electrokinetic effects, so-called electroviscous, viscoelectric, and axial electrokinetic development length effects, but this is not a major drawback since these effects are mostly additive to each other and their dependence on ionic and physical conditions are well explained in the literature.

In addition to electrokinetic effects on transport, velocity slip strongly affects the fluid flow in micro/nanoconfinements.[16,33−35] The emerging technologies include extremely smooth surfaces promoting slip depending on solid/liquid molecular interface coupling. Multiple numerical and theoretical studies explained that the hydrodynamic slip enhances the ion transport so the efficiency of related applications such as electrokinetic energy conversion.[28,35] Researchers also presented increased conduction current opposite to ionic current direction revealing itself as increased apparent viscosity (electroviscosity)[16,36−38] in case of slip, but overall flow rate and ionic current were found to still increase. For a liquid flow, the partial slip boundary condition was described by Navier[39] in 1823 and later acknowledged and validated by numerous researchers showing that the continuum solutions with Navier-slip condition yield accurate flow calculations for confinements as small as 3−4 nm.[10,35,40−45] Interface slip is defined as a function of two parameters: (i) slip length and (ii) velocity gradient at the interface.[46] First, slip length is proven to be a material property of the solid/liquid couple by many researchers.[46−51] Multiple studies relate the slip length to surface wetting and describe its variation by contact angle.[52,53] Surface electric condition is also found affecting the slip length,[16,17,54,55] but it actually develops at high surface charge values above the natural surface charging range. Second, velocity slip also depends on the near surface hydrodynamics that earlier mentioned electroviscosity and viscoelectic effects inside the EDL are expected to strongly alter, e.g., the boundary slip. Specifically, recent molecular dynamic (MD) simulations measure substantial decrease in slip length with increasing surface charge,[56,57] opposing earlier literature presenting negligible slip length change at the corresponding low surface charges.[58,59] Just recently, Rezaei et al.[56] presented that such discrepancy is due to neglecting local viscosity and the resulting velocity gradient near the surface, which is different than the bulk behavior. Slip length calculated from bulk velocity gradient is found to decrease, but if the local gradient is considered, slip length remains mostly constant at low surface charge values. Eventually, these studies measured decreasing velocity slip which is not due to change in slip length, but it is a result of viscosity change in the EDL. Hence, for a constant slip length and pressure gradient, velocity slip on surface varies by the change in electrokinetic effects which is mostly overlooked by the current literature. Specifically, such physical effects appear to be able to be estimated using a Navier-type boundary condition considering electrohydrodynamics.

Electrokinetic effects develop as a function of surface charge which is governed by the local ionic environment. Therefore, the EDL and surface charge are interrelated in nature. This behavior is commonly referred as the ***charge regulation*** (CR) nature of surface chemistry in the literature.[60−62] Most of the above given literature neglected CR and assumed a constant surface charge as a material property.[28,35,63] However, overlapping EDLs extending from opposite surfaces and ionic diffusion from reservoirs create deviation in ionic properties in the EDL from the descriptions of the Boltzmann distribution. Hence, ionic distribution and the resulting surface electric charge become functions of confinement *height* and *length* at nanoscales. Consequently, CR significantly effects the ion transport through nanofluidic systems. Recently, we characterized surface charge dependence on the corresponding channel length/height and ionic condition.[26]

For a correct ionic current estimation, electroviscous and viscoelectric effects with velocity slip under active charge regulation surface charge conditions should be considered in a coupled manner. As far as the authors' knowledge, the dependence of slip effects on varying effects of electroviscosity and viscoelectrics has never been analyzed using continuum solutions in the literature. Therefore, this study aims to resolve the ion transport through different length nanofluidic channels under the combined electroviscous, viscoelectric, and slip velocity effects with the CR model, unlike previous studies that focused on these physical effects, separately.

THEORETICAL BACKGROUND AND NUMERICAL MODEL

A pressure driven flow through a nanofluidic channel between two reservoirs is studied as illustrated in Figure 1. The liquid medium is a KCl electrolyte solution containing H^+, K^+, Cl^-, and OH^- ions whose bulk concentrations are denoted as C_{10}, C_{20}, C_{30}, and C_{40}, respectively. These ions are treated as point charges in the system. In order to ensure electroneutral conditions, the bulk concentration of ions are evaluated as C_{10}

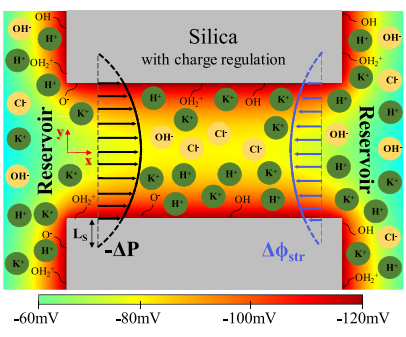

Figure 1. Schematic illustration of the solution domain.

https://dx.doi.org/10.1021/acs.langmuir.0c01457
Langmuir 2020, 36, 9191−9203

$= 10^{-pH+3}$, $C_{20} = C_{KCl} - C_{10} + C_{40}$, $C_{30} = C_{KCl}$, and $C_{40} = 10^{-(14-pH)+3}$. The debye length (λ), which is an indication of the EDL extension, can then be calculated as $\lambda = 1/\kappa = \sqrt{\varepsilon_0 \varepsilon_r k_B T / N_A e^2 \sum c_i z_i^2}$ where ε_0 and ε_r are the permittivity of vacuum and dielectric constants of electrolyte solution, k_B is the Boltzmann constant; T is the temperature; N_A is the Avogadro constant; e is the elementary charge, c_i and z_i and are the molar concentration and the valence of the ith ionic specie (i = 1 for H^+; i = 2 for K^+; i = 3 for Cl^-; i = 4 for OH^-) in the equation.

The transport of ions, electric potential, and velocity distribution within the domain are governed by the combination of Poisson−Nernst−Planck (PNP) and Navier−Stokes (NS) equations as follows:

$$-\varepsilon_0 \varepsilon_r \nabla^2 \psi = F \sum_{i=1}^{4} z_i c_i \tag{1}$$

$$\nabla \cdot \vec{N}_i = \nabla \cdot \left(-D_i \nabla c_i - z_i \vec{V} \frac{D_i}{RT} F c_i \nabla \psi + \vec{V} c_i \right) = 0 \tag{2}$$

$$\rho \frac{D\vec{V}}{Dt} = -\nabla P + \mu_E \nabla^2 \vec{V} + \vec{F_B} \tag{3}$$

Here, ψ is the electric potential, F is the Faraday constant, R is the universal gas constant, $\vec{N}_i$ is the flux density, D_i is the diffusivity of the ith ionic specie, ρ is the density of liquid solution, $\vec{F_B}$ is body force calculated from $\rho_V \, d\psi/dx$ where ρ_V is the charge density and $d\psi/dx$ is the potential variation in the flow direction. This term is the origin of the electroviscous effects created by the streaming potential. It should be noted here that the actual fluid viscosity is not altered and remains at the thermodynamic value, if only the electroviscous effects are considered (i.e., $\mu_E = \mu$). To solve the coupling governing eqs 1−3, we apply the following boundary conditions: The far ends of the two reservoirs are maintained at bulk ion concentrations (i.e., $c_i = c_{i0}$) while a pressure difference of ΔP is applied between them. On the channel walls, slip velocity develops (i.e., $u = u_{slip}$) develops with a surface charge of σ_w based on $-\varepsilon_0 \varepsilon_r (n \cdot \nabla \psi) = \sigma_w$ and the ion-impermeable condition (i.e., $-n \cdot \vec{N}_i = 0$). Here, n is the unit outer vector. At the side walls of the reservoirs, the no-slip condition (i.e., $u = 0$) with zero electric potential (i.e., $\psi = 0$) and ion-impermeable conditions are applied.

When the viscoelectric effects are included, the viscosity model defined by Dood and Andrade[23] is employed to calculated viscosity as a function of the electric potential variation in surface normal direction as

$$\mu_E = \mu(1 + fE^2) \tag{4}$$

In eq 4, μ is the bulk viscosity of liquid, E is the electric field strength normal to the flow direction, and f is defined as the viscoelectric coefficient. Here, electric field is due to the electric potential variation in surface normal direction as $d\psi/dy$. The value of viscoelectric coefficient, f, has been a controversial topic. In 1950, Dood and Andrade suggested that the viscoelectric constant ranges between 1×10^{-16} and 3×10^{-16} m^2/V^2 depending on the fluid type.[23] Seven years later, Hart[64] claimed to correct Dood and Andrade's study that proposed that viscoelectric constants have an error of 25% due to mistakes in their experimental procedure. In 1961, Lyklema and Overbeek[65] studied electroosmotic flows (EOF) theoretically and proposed the value of 1.02×10^{-15} m^2/V^2 for the viscoelectric constant, which is still *the most commonly employed value for f* in the literature. Yet, there are many studies claiming that f should be lower, on the order of 10^{-17} m^2/V^2.[66,67] Starting in the 2000s, MD simulations have been performed for EOF through nanochannels[68,69] and increases in local viscosity were observed near the charged surfaces up to 5 times of its bulk value.[68] Similarly, Qiao and Aluru[70] studied EOFs and concluded that viscosity increased near the surface as a result of the electric field normal to flow direction. In a very recent MD study by Hsu et al.,[25] they calculated the viscoelectric constant of 2.3×10^{-16} m^2/V^2, which is also very close to the earlier experimental results of Hunter and Leyendekkers.[71] Overall, the debate on the accurate value of viscoelectric constant continues within a range of 10^{-17} to 10^{-15} m^2/V^2. The reason for such a wide range of values develops since multiple mechanisms affecting viscoelectric physics are simply incorporated into eq 4 through the viscoelectric coefficient, f. For example, variation in solid/liquid coupling, the type of liquid, ionic sizes, and even permittivity play major roles on the viscoelectric effects. In such a case, Bazant et al.[72] proposed a power law equation to model the ion size and permittivity effects called as charge-induced thickening in eq 5.

$$\frac{\varepsilon}{\mu_E} = \frac{\varepsilon_b}{\mu} \left[1 - \left(\frac{|\rho_V|}{\rho_{V,max}} \right)^{\alpha} \right]^{\beta} \tag{5}$$

where α and β are the exponents as the fitting parameters to model various experimental and simulation conditions. The ρ_V is the local charge density and $\rho_{V,max}$ is the steric constraint of the Modified-Poisson−Boltzmann model proposed by Bikerman.[73] The steric constant can be calculated by ze/a^3, where z is the valence, e is the elementary charge, and a is the effective size parameter related to ion diameter (d) through $a^3 = 0.83d^3$.[74] Bazant et al.[72] combined charge-induced thickening with viscoelectric effect and introduced a hybrid model. They defined the variation in permittivity negligible based on the MD calculations[68,69] and also selected $\alpha = 2$.

$$\mu_E = \mu \left[1 - \left(\frac{|\rho_V|}{\rho_{V,max}} \right)^2 \right]^{-\beta} (1 + fE^2)^{\gamma} \tag{6}$$

Here, Bazant et al. also introduced γ to combine viscoelectric effect with charge-induced thickening. Recently, Celebi et al.[45] employed eq 6 to describe their MD measurements; they calculated the viscosity parameters as constant values of $\beta = 4$ and $\gamma = 1.6$ in the Debye−Huckel region, where surface charge is lower than -0.1 C/m^2. We aimed to adopt the accurate description of eq 6 with parameters calculated from the MD simulations. For such a case, we incorporated the above given different mechanisms into the single parameter of f based on eq 4, similar to earlier literature. In Figure 2, we presented the viscosity distribution estimated by eq 6 using corresponding parameters from the MD results[57,72] (d = 0.4 nm, $\beta = 4$, and γ = 1.6) with the most common $f = 1 \times 10^{-15}$ m^2/V^2[65] based on the local charge density calculated by PNP for the 10 nm height channel at 10 mM. Next, we calculated the f value for eq 4 to estimate a similar viscosity variation for the same charge density distribution. We found finite-size ion effects can be

https://dx.doi.org/10.1021/acs.langmuir.0c01457
Langmuir 2020, 36, 9191−9203

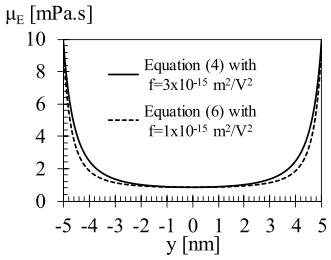

Figure 2. Comparison of local viscosity variation calculated by the viscoelectric model (eq 4) with $f = 3 \times 10^{-15}$ m^2/V^2 and the hybrid model (eq 6) $f = 1 \times 10^{-15}$ m^2/V^2.

incorporated into viscoelectric calculations of eq 4 with $f = 3 \times 10^{-15}$ m^2/V^2 which are used in the current study.

Next, velocity slip was applied at the nanochannel walls using the following Navier slip boundary condition as

$$u_{slip} = L_s \left.\frac{du}{dy}\right|_{wall} \tag{7}$$

Equation 7 describes the tangential liquid velocity at the interface as a function of the slip length, L_s, and the velocity gradient in surface normal direction. As explained earlier, L_s is defined as a material property of the given liquid/solid couple by many researchers. Lyklema[75] extended this knowledge by presenting the charge dependency of slip length in 1994. Later, Joly et al.[54] proposed an equation for the charge dependent slip length based on their MD study[44] in 2004. Starting from the Green−Kubo relation for friction coefficient, they separated the van der Waals and Coulombic contributions. Jing and Bhushan[58] implemented this slip length formula to their theoretical model and investigated the slip effect on the pressure driven flow in micro- and nanoscale channels. They showed that slip length can vary significantly depending on the surface electric charge. However, in 2013, Pan and Bhushan[59] experimentally studied the effect of surface charge on slip length through atomic force microscopy (AFM) measurements. They presented that the formula proposed by Joly et al. is accurate, except a missing factor of l/d at the second item in the denominator, which has been corrected as

$$L_s = \frac{L_{s,0}}{1 + (1/\alpha)(\sigma d^2/e)^2 (l_b/d^2) L_{s,0}} \tag{8}$$

In this equation, $L_{s,0}$ is the slip length in the absence of surface charge, α is a numerical factor ($\approx$1), σ is the surface charge, and d is the solid molecular diameter. l_B (Bjerrum length) is the separation at which the electrostatic interaction between two elementary charges is comparable in magnitude to the thermal energy scale. Bjerrum length is defined as $l_B = e^2/(4\pi\varepsilon_0\varepsilon_r k_B T)$ where e denoting the elementary charge, ε_0 and ε_r are the permittivity of vacuum and dielectric constants of electrolyte solution, k_B is the Boltzmann constant; T is the temperature. In water at room temperature, the Bjerrum length can be estimated as l_B = 0.7 nm.[54] Equation 8 has been employed in many AFM studies for various surface/liquid couples.[76,77] We also used eq 8 with $L_{s,0}$ = 5 nm, which is an average value for silica/water interfaces.[46,78]

The coupled behavior of the local ionic concentration in the electrolyte solution and the surface dissociation/association reactions creates the surface charge. This spontaneous phenomenon is commonly simulated by charge regulation models[26,79−85] in the literature. In the case of silica channel walls, the resulting surface charge can be evaluated through the following equations.

$$SiOH \leftrightarrow SiO^- + H^+ \tag{9}$$

$$SiOH + H^+ \leftrightarrow SiOH_2^+ \tag{10}$$

$$K_A = \frac{\Gamma_{SiO^-}[H^+]_w}{\Gamma_{SiOH}}; \quad K_B = \frac{\Gamma_{SiOH_2^+}}{\Gamma_{SiOH}[H^+]_w} \tag{11}$$

$$\sigma_w = -\frac{F\Gamma_{total}}{N_A} \frac{K_A - K_B[H^+]_w^2}{K_A + [H^+]_w + K_B[H^+]_w^2} \tag{12}$$

K_A and K_B in eq 11 are the equilibrium constants of surface reactions shown in eqs 9 and 10. These reactions are assumed to be instantaneous and occur much faster than the transport of ions, which is a consistent assumption since the Damkohler number in the current system is greater than 1 ($Da \gg 1$). Moreover, Γ_{SiO^-}, Γ_{SiOH}, and $\Gamma_{SiOH_2^+}$ symbolize the site densities of functional groups on the silica surface and $[H^+]_w$ is the hydrogen ion concentration at the solid/liquid interface.

The PNP and Navier−Stokes equations are solved numerically with CR in two-dimensional Cartesian coordinates using the commercial finite-element package, COMSOL Multiphysics (www.comsol.com). For the model parameters, we used the following values: ε_0, ε_r = 7.08 × 10^{-10} F/m, R = 8.31 J/(mol·K), F = 96485 C/mol, T = 300 K, N_{total} = 4.816 1/nm^2, pK_A = −logK_A = 7, and pK_B = −logK_B = 1.9. These parameters employed also by other researchers[86,87] are validated by experiments in our earlier study.[88] The diffusivity values of 9.31 × 10^{-9}, 1.957 × 10^{-9}, 2.032 × 10^{-9}, and 5.3 × 10^{-9} m^2/s are used for H^+, K^+, Cl^-, and OH^- ions, respectively[89] while pH is kept constant at 7.5.

The fluid flow is created by applying different pressures from the opposing reservoirs. The pressure gradient was kept constant through the channels by adjusting the inlet and outlet pressures of different length channels. In the integral form, volumetric flow rate is calculated as the function of velocity profile in x-direction as

$$Q = 2w\rho \int_0^{h/2} u(y)\, dy \tag{13}$$

The ionic current is the function of x-direction velocity profile and the ionic density profile as

$$I = 2w \int_0^{h/2} \rho_V(y) u(y)\, dy \tag{14}$$

In the absence of electrokinetic forces, eq 3 with slip boundary conditions can be solved and the following velocity profile will be obtained.

$$u(y) = \frac{1}{2\mu}\frac{dP}{dx} H^2 \left(\frac{y^2}{H^2} + \frac{L_s}{H} - \frac{1}{4}\right) \tag{15}$$

The solution system is validated analytically by Mei et al.[90] who developed a closed form solution for ionic current, starting from nonlinear Poisson−Boltzmann (PB) and Navier−Stokes (NS) equations by considering the charge regulation nature of surfaces. Mei et al. simply consider a fundamental system at equilibrium of ionic current, streaming potential, and conduction current. Using our model, we simulated a channel with 10 height and 300 nm length at the

https://dx.doi.org/10.1021/acs.langmuir.0c01457
Langmuir 2020, 36, 9191−9203

conditions employed in Mei et al. We should note here that the analytical solution from ref 90 had no channel length dependence, so we simulated 300 nm length channel which was found long enough to develop length independent results. Furthermore, both viscoelectric and velocity slip effects are not included in the solution of ref 90 since we kept viscosity constant independent from ionic conditions and used no-slip boundary conditions on surfaces as $L_{s,0}$ = 0 in this validation run. Only electroviscous effects exist in analytical solution, so we only had electroviscous effects in our validation runs. In Figure 3a, we compared the volume charge density and

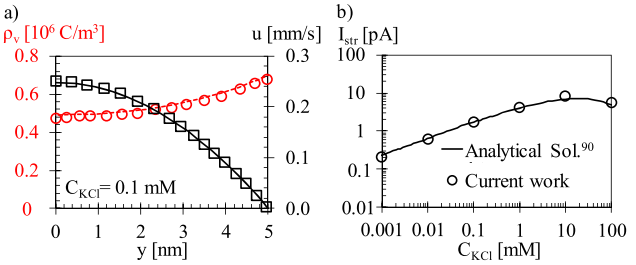

Figure 3. Comparison of the current simulation results of (a) velocity and ionic distribution in the channel at 0.1 mM salt concentration and (b) developed ionic currents at varying salt concentration with the analytical solution of Mei et al.[90] Solid lines are the solution of ref 90 while the markers represent the results of our model.

velocity profile results of our model in half of the channel with the analytical solution of Mei et al. for a 0.1 mM salt concentration, pH 7.5, and pressure gradient of 20 Pa/nm. The results display a perfect match. Using the ionic distributions and velocity profiles, ionic currents at different ion concentrations of 0.001, 0.01, 0.1, 1, 10, and 100 mM were calculated using eq 14. Comparison of current simulation results with the results of Mei et al. given in Figure 3b also showed good agreement.

RESULTS AND DISCUSSION

Starting from the validation with the analytical solution from ref 90, we systematically included viscoelectric and slip effects into solution by using eqs 4 and 7. First, we focused on the velocity profiles of each case considering different effects. We studied a 10 nm height and 100 nm length channel with a pressure gradient of 92 Pa/nm between the channel ends. In Figure 4, the corresponding normalized velocity profiles at the middle of the nanochannel length away from inlet and exit regions are presented at varying salt concentrations of 0.42, 0.94, and 10 mM. Figures 4a–c are normalized with the averaged velocity developing in a simple pressure driven flow known as Poiseuille flow (PF) without any electrokinetic and slip effects. As a first step, when the advection of ionic species was considered, pressure driven flow creates the conduction current that velocities became lower than the PF predictions. This is the so-called electroviscous effects. Electroviscous effects are mostly characterized by the EDL overlap. Through the concentration range we studied, EDL thickness changes between 1.5 to 15 nm; we did not observe a distinct variation in electroviscosity with variation in salt concentration inside the current 10 nm height channel for the no-slip case.[16] Next, we included the viscoelectric effects. Velocity profiles revealed local variation of viscosity near the surface especially for bulk concentrations of 10 mM, where the velocity profile becomes almost flat at the near wall regions. Velocities decreased due to viscoelectric effects. As a final step, we added velocity slip as defined as in eq 7 with a slip length of 5 nm. Slip on surfaces has a positive effect on transport as the fluid velocities increase. However, this flow enhancement develops a lot less compared to the nonionic regular PF case, since the velocity slip values on the surface show significant dependence on electrokinetic effects, which alters the near-wall hydrodynamics. First, electroviscous effects alone decrease the velocity gradient near the surface as a result of the reverse ionic flow due to streaming potential that velocity slip on surface decreases. The addition of viscoelectric effects further lessens the velocity gradients and the resulting velocity slip. This behavior also shows dependence on ionic conditions; with an increase of salt concentration, velocity slip on the surface decreases. The major influence on velocity slip develops due to viscoelectric effects. An almost 30% decrease of velocity develops at even a very low

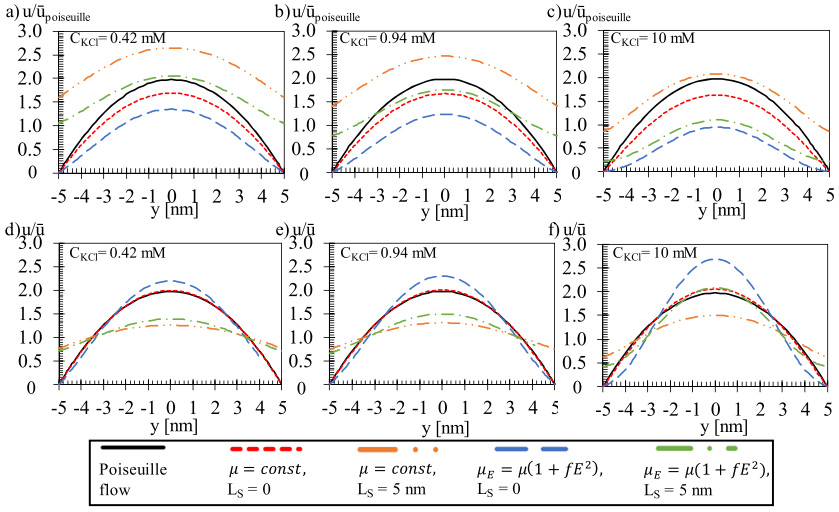

Figure 4. Velocity profiles along the channel height under different effects and at different salt concentrations. Velocities were normalized (a, b, and c) with the average velocity of the simple pressure driven (Poiseuille) flow solution and (d, e, and f) with the average velocity of corresponding case.

https://dx.doi.org/10.1021/acs.langmuir.0c01457
Langmuir 2020, 36, 9191−9203

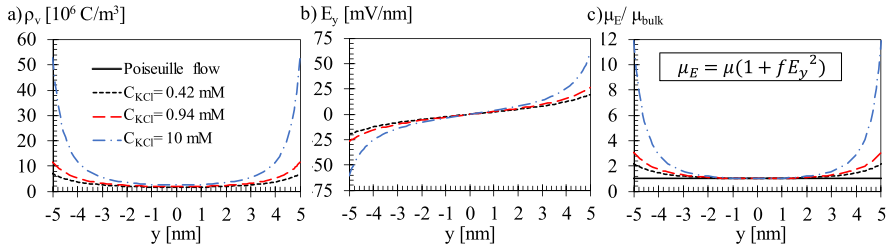

Figure 5. Distribution of (a) volume charge density, (b) electric field, and (c) normalized local viscosity along the channel.

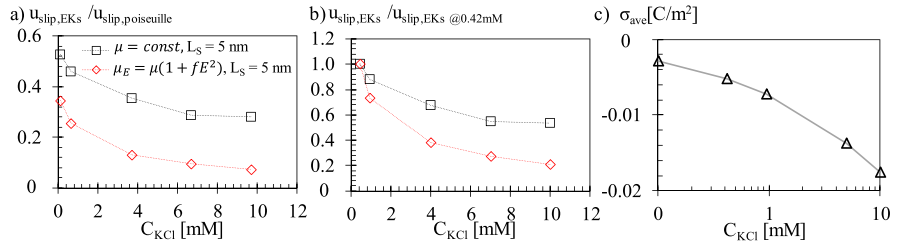

Figure 6. Variation of velocity slip on surface normalized by (a) the Poiseuille flow velocity slip and (b) velocity slip measured at the 0.42 mM case. (c) Silica surface charge as a function of salt concentration based on charge regulation.

ionic concentration of 0.42 mM, while an almost no-slip (~80% decrease) condition develops in the 10 mM case.

Next, we normalized the velocity profiles with their own average values, in order to compare the shape of velocity profile of different cases. The results are depicted in Figures 4d–f. A fully developed pressure driven flow yields a velocity profile in a perfect parabolic shape. For the cases where electroviscous effects were considered only, velocity profiles remained almost parabolic even at high salt concentrations. Yet, when viscoelectric and slip effects were considered, the shape of velocity profiles became different than a parabola while near surface distributions are even flattened. In order to understand the viscoelectric effects, we studied the distribution of volume charge density and the resulting electric field strength along the channel center in Figure 5a and b, respectively. Due to ionic layering in the EDL, charge concentration near the surface increases exponentially. With an increase in salt concentration, surface charge and the resulting ionic accumulation at opposite sign increase. Charge concentration decays and reaches zero sufficiently away from surface at the channel center as the number of negative and positive ions becomes equal. For diluted solutions, thick EDL is formed near the surface but its effect on the fluid reduces. Therefore, thinner EDL thickness yields higher electrostatic interactions. Due to the local electric potential gradient, there forms an electric field in the surface normal direction as given in Figure 5b. Compared to lower concentrations (0.42 and 0.94 mM), the volume charge density increases up to 5-fold at 10 mM while the electric field doubles its strength due to the highly condensed and strong ionic layering near the surface at high salt concentrations. As a result of variation of ionic concentration, the viscosity of the electrolyte varies in the surface normal direction. Figure 5c presents the distribution of viscosity normalized with bulk viscosity at the channel center based on the description of eq 4. The local viscosity can reach up to 10–12 times its bulk value near the surface. The difference between near surface viscosity and bulk viscosity increases with increase in salt concentration.

Later on, we measured the velocity slips developed on surface at different ionic conditions for the prescribed constant slip length and pressure gradient. Figure 6a presents variation of surface velocity slip compared to the value developing at the simple pressure driven flow condition. We studied slip velocities in two cases: (i) ionic flow with electroviscous effects and constant viscosity and (ii) ionic flow with both electroviscous and viscoelectric effects. For both cases, velocity slip on the surface is lower than the PF velocity slip and decreases with the increase of salt concentration. In the first case, electroviscous effects create conduction current opposite to the flow direction which is more profound in the near surface EDL region and alters the velocity gradient on the surface. Hence, slip velocity decreases, for a constant slip length condition. In the second case, further flow retardation develops as the viscoelectric effects create higher local viscosity resisting the motion of fluid particles. The deviation of the slip velocity from the PF estimations becomes higher when the viscoelectric effects were incorporated into the analyses. In both cases, decrease of velocity slip becomes more prominent with the increase of salt concentration as the decrease in EDL thickness creates higher gradients. For the case where both electroviscous and viscoelectric effects are included, almost a no-slip condition develops at a salt concentration of 10 mM. Decrease of the slip velocity by increasing the salt concentration becomes negligible for salt concentrations higher than 7 mM where the ratio of EDL thickness to channel height (λ/H) becomes higher than 0.73. Based on this fact, we kept the studied concentration in the current range. ***These results suggest that the possible effects of boundary slip on fluidic transport should not be characterized simply based on slip length value.*** We compared the velocity slip variation by salt concentration in these two cases in Figure 6b. Velocity slip values were normalized by the velocity slip measured at the lowest salt concentration studied (0.42 mM) at which the lowest deviation from PF slip velocity is observed. While the velocity slip decreases as the salt concentration increases, this decrease is much more dominant for the second case where both electroviscous and viscoelectric effects were considered. In Figure 6c, we present the silica surface charge at the corresponding salt concentrations developed based on the natural "charge regulation" behavior. Simply, the absolute value

https://dx.doi.org/10.1021/acs.langmuir.0c01457
Langmuir 2020, 36, 9191–9203

of the surface charge increases with increasing ion concentration, which is identical to theoretical calculations.

The above findings are very similar to physics observed by multiple MD studies from the literature. However, the observed variation in velocity slip is attributed to the change of slip length in most of these studies. Although slip length shows variation depending on the surface charge as described in ref 54 in detail, this variation originates due to change in electrostatic forces altering interfacial coupling, which eventually remains constant at low surface charges within the charging range of natural surface chemistry. Hence, change of slip velocity by the increase of surface charge in this range is not due to change of slip length; instead, it is due to change in near surface electrohydrodynamics. Recently, Rezaei et al.[56] conducted shear driven flow MD simulations and calculated two different slip lengths based on local and bulk velocity gradients. In Figure 7a, we present these local and bulk slip

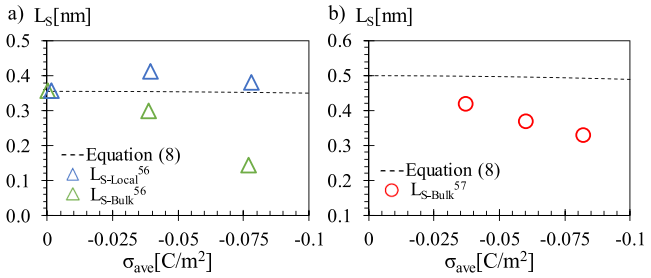

Figure 7. Variation of slip lengths by surface charge measured by MD simulations (markers) from (a) Rezaei et al.[56] and (b) Celebi et al.[57] compared with the estimation of eq 8 from Joly et al.[54] (dashed lines).

lengths as a function of surface charge, in comparison with the predictions of eq 8. While the bulk slip length shows a substantial decrease by increasing surface charge, local slip length remains almost constant, similar to the calculations of eq 8. We can also show a similar behavior from an another recent MD study by Celebi et al.[57] who eventually described viscoelectric effects to a great extent using eq 6. They also related the measured velocity slip change to change of slip length in the low surface charge Debye−Huckel region, while slip length predictions of eq 8 remain constant for the corresponding surface charges (Figure 7b). Hence, change of velocity slip on surface is not due to change of slip length, but it is a result of near surface electrohydrodynamics.

MD simulations naturally create both the interface coupling and the near-wall hydrodynamics. Here, we employed the spatial viscosity variation described in Celebi et al.'s MD work (Figure 2) and obtained decrease of velocity slip with increasing ionic concentration (increasing surface charge), which is also similar to their MD findings. The current results simply show that the momentum equilibrium between surface and liquid measured by MD simulations can be estimated using a continuum solution with Navier-type boundary condition if the electrohydrodynamics based on electroviscous and viscoelectric effects are included.

Next, we calculated the ionic currents using eq 14. Figure 8 presents the variation of ionic current by KCl concentration (0.1, 0.42, 0.94, 5, and 10 mM at pH = 7.5) for the cases where different effects were considered. In order to compare our results with Mei et al.,[90] we utilized corresponding parameters from their study. Overall, ionic current increases with an increase salt concentration due to decreased electroviscosity

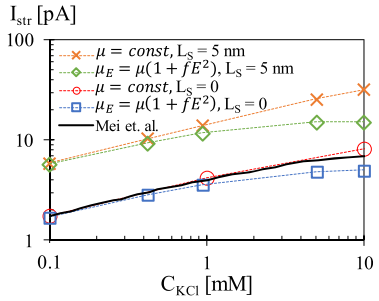

Figure 8. Ionic current of the electroviscous flows with and without viscoelectric and velocity slip effects as a function of salt concentration.

effects (conduction current) and increased ionic concentration, as expected. Our calculations with no viscoelectric and slip effects show good match with the results of Mei et al.[90] as discussed earlier. With the addition of viscoelectric effects, the ionic current decreases, which becomes substantial for ionic concentrations higher than 1 mM. At 10 mM, the ionic current decreases to 70% of the prediction of Mei et al. With increased concentration, the absolute value of electric charge developed on surface increases resulting in a stronger electrical field strength in surface normal direction. This causes the local viscosity to increase near wall regions according to eq 4, which in return decelerates the movement of ions due to higher shear forces. Hence, the deviation of results presented by square markers from the circle markers at elevated salt concentrations arises solely from the viscoelectric effect. Next, the velocity slip effect is included in cases with and without the viscoelectric effect. It should be noted that, in the current range of surface charge according to natural CR behavior, surface charge has almost no effect on slip length described by eq 8 that slip length remained a constant material property. The highest surface charge at 10 mM is in the order of 10^{-2} C/m^2. Earlier literature showed that charge density should be higher than 10^{-1} C/m^2 in order to affect the slip length.[58,59] Therefore, we continued with a constant slip length value of 5 nm.

Overall, velocity slip on the wall significantly increased the ionic transport even at this moderate slip length value.[16,46] Without viscoelectric effects, ionic current continues to increase as the salt concentration increases, similar to the no-slip condition. Here, velocity slip decreases with an increase in salt which also results in a decrease of electroviscous effects, such that corresponding decreasing and increasing effects on ionic current remained in balance with each other. However, when the viscoelectric effects were added, ionic current enhancement substantially reduces by the increase of salt concentration. This is due to the dominant decrease of the velocity slip presented in Figure 6. This is an expected outcome as the slip velocity depends on the velocity gradient at the solid/liquid interface for a given slip length while the velocity gradient varies with local changes in the viscosity as a result of electrokinetic effects. This is overlooked in the literature. Hence, the slip velocity shows variation by the change in the ionic condition even if the slip length is a constant property for a given liquid/solid couple and surface charge; which is indeed one of the main focuses of the current study.

Many studies in the literature also focus on the short channels, claiming that the electrokinetics within these channels substantially vary from longer channels where the

https://dx.doi.org/10.1021/acs.langmuir.0c01457
Langmuir 2020, 36, 9191−9203

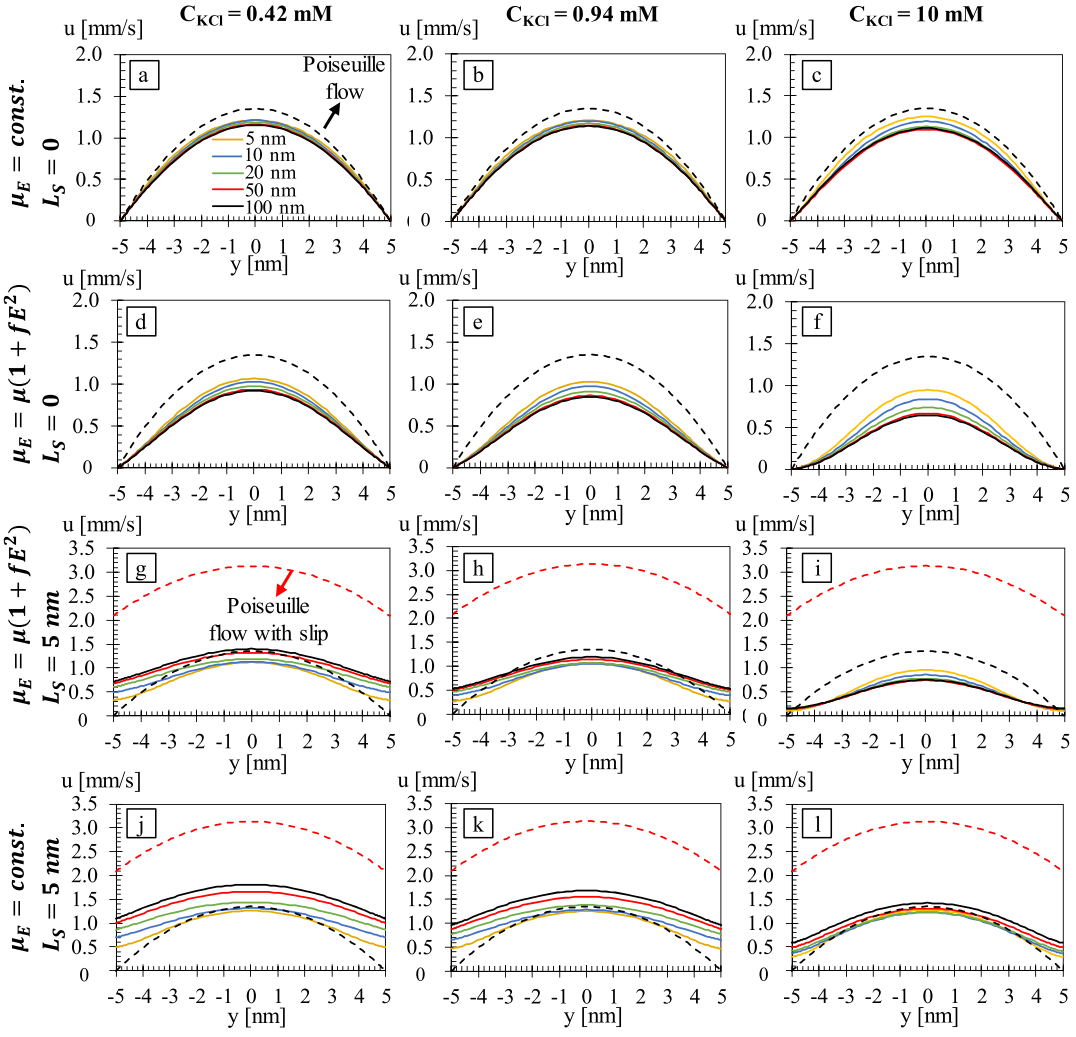

Figure 9. Velocity profiles along the channel height measured at the middle of 5, 10, 20, 50, and 100 nm length channels at KCl concentrations of 0.42 mM (a, d, g, j), 0.94 mM (b, e, h, k), and 10 mM (c, f, i, l) in the cases where different electrokinetic effects were considered.

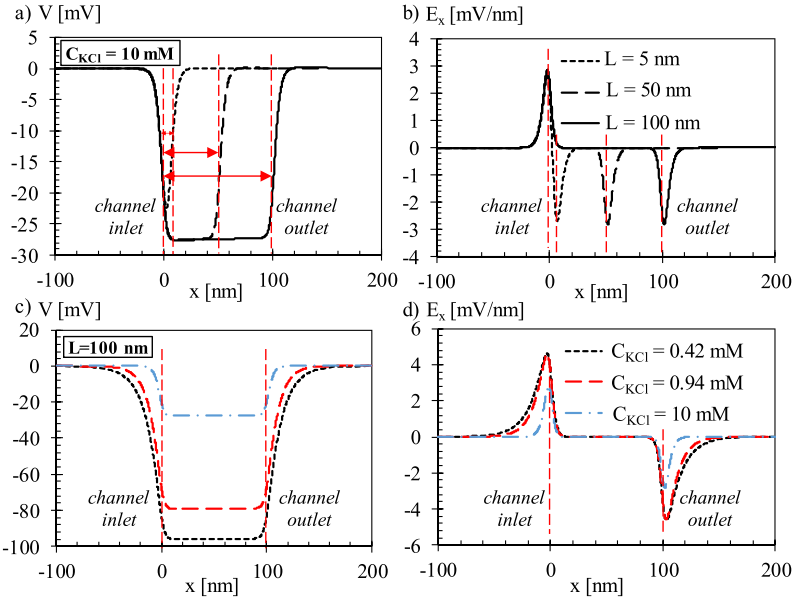

Figure 10. (a) Electrical potential and resulting (b) electric field strength variation along the centerline for different length channels at salt concentrations of 10 mM. (c) Electrical potential and resulting (d) electric field strength variation along the centerline for different salt concentrations in the 100 nm long channel.

https://dx.doi.org/10.1021/acs.langmuir.0c01457
Langmuir 2020, 36, 9191−9203

inlet/outlet effects can be safely ignored.[29,30,32] Hence, we further extended our study to the length dependence of ionic transport. Different length nanofluidic channels were studied under different electrokinetic conditions and effects. In Figure 9, velocity profiles measured at the middle of the nanochannel for channel lengths of 5, 10, 20, 50, and 100 nm are presented for KCl concentrations of 0.42, 0.94, and 10 mM. The first row of figures (Figure 9a–c) presents velocity profiles with electroviscous effects only compared to simple PF case with no electrokinetics. By decreasing channel length at a certain concentration, velocity increases due to decreasing streaming potential and its retarding effect, especially at low concentrations.[31] The ionic concentration inside the channel is different than the reservoir such that an ionic concentration gradient develops in the axial direction between the channel and reservoir at the channel inlet and outlet.[26] Also called "electrokinetic development length," ionic concentration inside a channel reaches its equilibrium value sufficiently away from reservoir connections. If a channel is shorter than this electrokinetic entrance length, the ionic conditions inside the channel will be different. Here, channel length and bulk ionic concentration are two determining parameters that we examined in Figure 10. The axial electric potential distribution and resulting electric field along the line passing through the channel center are presented in Figure 10a and b for channel lengths of 5, 50, and 100 nm at 10 mM salt concentration. It can be observed that the 5 nm channel length is smaller than the entrance length from the inlet and outlet and that lower electric potential difference (Figure 10a) between the channel and reservoir develops, which ultimately creates a lower electric field difference as seen in Figure 10b. Therefore, lower streaming potential develops and the ionic current experiences less resistance at short channels.[31] Next, we varied the bulk concentration for a 100 nm-length channel. The corresponding electric potential and electric field are presented in Figure 10c and d. As the concentration increases, EDL thickness reduces and ionic concentration difference between channel and reservoirs decrease. Hence, the electric field resulting from the potential bias is lower at 10 mM. On the other hand, very high osmotic pressure builds up at the channel entrances at low concentrations that creates entrance resistance at the channel ends. This makes the nanofluidic channels so-called ion selective.[32]

In the second row (Figure 9d–f), viscoelectric effects are added to the electroviscous effects, which develop further retardation of flow. It appears that viscoelectric effects have a higher length dependence and that decrease in the channel length result in an almost 40% increase in velocity from 100 to 5 nm-length channels at 10 mM. On the other hand, the flow is suppressed more near the wall regions for higher concentrations as a result of viscoelectric effects. This is due to the increase of surface charge due to inlet/outlet effects,[26] which creates further ionic layering and increase in the local viscosity in those regions. The interesting consequence of this behavior shows itself in the case of slip condition. The third row of figures (Figure 9g–i) presents results with the addition of velocity slip at a constant slip length of 5 nm. One would expect the velocity distributions shown in Figure 9d–f to just shift upward by the velocity slip. However, Figure 9g–i shows otherwise; in addition to variation of velocity slip by concentration given in Figure 6, slip velocity also shows a strong dependence on channel length. Velocity gradient at the surface varies due to variation of electroviscous and viscoelectric effects by channel length. Divergence from simple Poiseuille estimations with slip becomes enormous. Excluding viscoelectric effects creates a slight change in results, mostly at high ionic concentration where viscoelectric effects were strong as shown in Figure 9j–l. Velocity slips slightly increase.

Variation of velocity slip by channel length is given in Figure 11 at different salt concentrations. Figure 11a and b presents

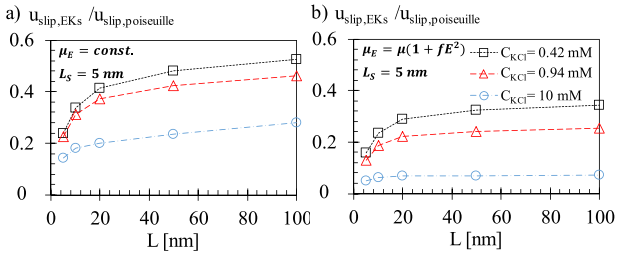

Figure 11. Velocity slip at the wall (a) without and (b) with inclusion of viscoelectric effects.

the velocity slips without and with viscoelectric effects, respectively. Overall, velocity slip decreases by decreasing channel length. This length dependence is more dominant at lower concentrations. By addition of viscoelectric effects in Figure 11b, velocity slips values decrease 40% more. Figure 11b reveals that velocity slip becomes independent from channel length for $L > 20$ nm.

As a final step, we calculate the flow rates (eq 13) and the ionic current (eq 14) through different length channels at varying salt concentration in Figure 12. The mass flow rates normalized with the PF estimations are given in Figure 12a for different channel lengths and concentrations. First, considering electroviscous effects alone yields lower flow rates than PF while low channel length and salt concentration dependency develops. Only at very short channel length of 5 nm,

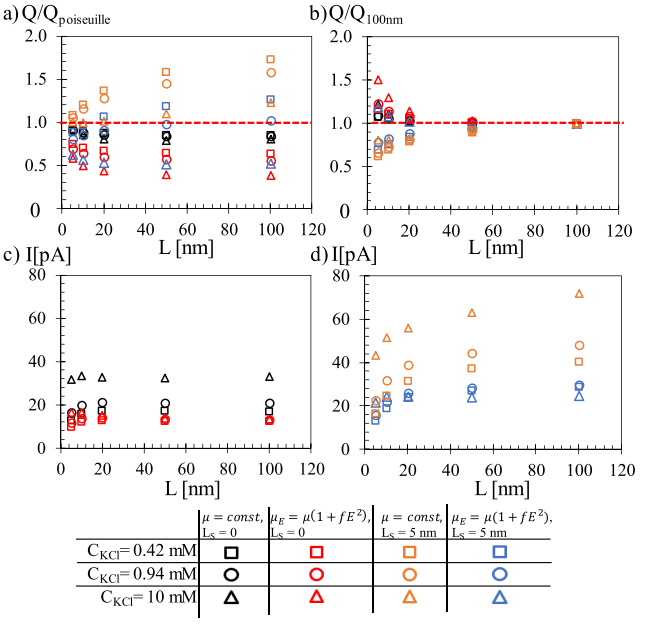

Figure 12. Flow rates of different length channels (a) normalized by Poiseuille flow (PF) calculation and (b) normalized by the results of a 100 nm length channel. Ionic currents (c) without and (d) with the slip effect.

https://dx.doi.org/10.1021/acs.langmuir.0c01457
Langmuir 2020, 36, 9191–9203

conduction current become almost negligible and since shorter channels have small resistance at the channel entrances as already discussed in Figure 10, flow rates approach back to PF value for the same applied pressure gradient. When we include the viscoelectric effects, mass flow rate further decreased; higher length and salt concentration dependency develop. Overall, flow rates lower than simple pressure driven flow (PF) develop under electroviscous and viscoelectric effects, but these effects lessen with a decrease in salt concentration and/or decrease in channel length.

When the slip boundary condition is included, flow rates increase. The case with electroviscous effects alone developed an almost 70% higher flow rate than PF for 100 nm long channel at low salt concentration. However, velocity slip and resulted flow enhancement decreases as salt concentration increases and/or channel length decreases. Especially by the inclusion of viscoelectric effects, velocity slip on boundary shows a substantial decrease and flow rate approaches back to results of the no-slip condition. We should note here that L_s = 5 nm represents an average slightly hydrophobic surface with wetting contact angle around 90°.[91] Eventually, having such a slip condition without any electrokinetics yields almost a 3 times increase in flow velocity and more than a 5 times increase in mass flow rate, for a simple PF case. However, this flow enhancement due to boundary slip does not develop in the case of a flow with electrokinetic effects, especially in short channels and/or at high salt concentrations. For example, almost no flow enhancement developed for 10 mM case of L_s = 5 nm with electroviscous and viscoelectric effects (velocity profile in Figure 9i), and flow rate remained at half of the PF value for all channel lengths. In the 0.94 mM concentration case, the velocity slip can only balance the reduction in the flow rate from electroviscous and viscoelectric effects if the flow rate reaches back to the PF value for channel lengths higher than 50 nm.

In order to understand the effect of channel length better, we normalize flow rate values with the flow rate measured in longest channel case of 100 nm in Figure 12b. There is only a slight change in flow rate between 50 and 100 nm long channels; therefore, we can consider 100 nm as a length independent case. Decrease in channel length increases the flow rate of no-slip cases while the opposite behavior develops when boundary slip included. Flow rate decreases by the decrease of channel length for slip cases. This is due to opposite effects developing; decrease of channel length decreases electrokinetic retardation effects on flow, but in the case of a slipping boundary, it also decreases velocity slip and flow enhancement.

Ionic transport resulting from these pressure driven electrokinetic flows without and with velocity slip are given in Figure 12c and d, respectively. When the electroviscous effects were considered alone, ionic current increases with an increase in salt concentration. This behavior is actually opposite of the salt concentration dependence on flow rate. Increasing the salt concentration increases the electrokinetic effects obstructing the flow and reducing the flow rate, but it also increases the number of ions in the channel that ionic conduction actually increases even though the flow rate decreased. Multiple researchers observe a similar behavior and conclude that ionic current enhances with an increase in salt concentration.[31,60,62,92] However, when the viscoelectric effects are included, the ionic current becomes almost independent of salt concentration except for very short channels and very low salt concentrations, which is a very interesting outcome. It appears that the negative and positive influences of increased ion concentration basically cancel each other since increased ion concentration also enhances the strength of viscoelectric effects. Without velocity slip, there is very low channel length dependency developing in ionic current. When the slip condition is included, velocity slip enhances the ionic current, but its influence was lower under viscoelectric effects. This validates that electroviscous and viscoelectric do not only affect the ionic current directly, but a prominent length dependent variation develops originating from the variation of velocity slip by channel length. When both electroviscous and viscoelectric effects are considered, ionic current becomes independent of slip and salt condition in short channels (L < 5 nm).

CONCLUSION

We studied the ionic currents of pressure driven flows in nanofluidic channels with varying salt concentration and channel length. For the first time in the literature, the influence of the slip boundary condition is described under both electroviscous and viscoelectric effects. By validating the calculation procedure with the analytical solution for the ionic current with electroviscous effects,[90] we present that further including the viscoelectric effects and boundary slip creates significant variations in the ionic transport. Simply, results show that electroviscous and viscoelectric effects decrease the transport due to conduction current and increase in local viscosity. Different than the earlier studies presenting increasing ionic current by increased salt concentration, ionic current is found to be independent of salt concentration, except for very short channels and very low salt concentrations, when the viscoelectric effects are considered in addition to the electroviscous effects. In the case of no-slip, decreasing the channel length increases the volumetric flow rates but, at the same time, decreases the equilibrium ion quantity forming inside the channel and ionic current shows almost no channel length dependency. When the slip condition is added, ionic conduction is enhanced. Even though we apply a constant slip length, the velocity slip value on surfaces shows significant variation with the salt concentration, channel length, and electrokinetic effects included in the solution. We compare and validate the observed behavior with the results of MD calculations from multiple studies. While the MD naturally simulates both the interface coupling and the near-wall hydrodynamics, we show that similar physics can be estimated using a continuum solution with Navier-type boundary conditions if the electrohydrodynamics based on electroviscous and viscoelectric effects are included. Considering electroviscous effects alone yields up to 70% lower velocity slips than Poiseuille flow predictions while further adding viscoelectric effects creates almost a no-slip condition at high salt concentrations. Velocity slip also shows strong dependence on channel length; decreasing length yields decreasing velocity slip on the surface. Hence, ionic current lessens profoundly with the decrease in channel length.

AUTHOR INFORMATION

Corresponding Author

Murat Barisik − *Department of Mechanical Engineering, Izmir Institute Of Technology, Izmir 35430, Turkey;* orcid.org/0000-0002-2413-1991; Email: muratbarisik@iyte.edu.tr

https://dx.doi.org/10.1021/acs.langmuir.0c01457
Langmuir 2020, 36, 9191−9203

Author

Tumcan Sen − *Department of Mechanical Engineering, Izmir Institute Of Technology, Izmir 35430, Turkey*

Complete contact information is available at: https://pubs.acs.org/10.1021/acs.langmuir.0c01457

Notes

The authors declare no competing financial interest.

■ ACKNOWLEDGMENTS

This work was supported by the Scientific and Technological Research Council of Turkey (TÜBİTAK) under the Grant Number 118M710. This work was also supported by the BAGEP Award of the Science Academy. The authors would like to thank the Center for Scientific Computation at Southern Methodist University and Dr. M. Polat and Dr. U. Ozkol for their useful discussions and insightful remarks.

■ REFERENCES

(1) Zhang, B.; Wood, M.; Lee, H. A silica nanochannel and its applications in sensing and molecular transport. *Anal. Chem.* **2009**, *81* (13), 5541−8.

(2) Ryzhkov, I. I.; Minakov, A. V. Theoretical study of electrolyte transport in nanofiltration membranes with constant surface potential/charge density. *J. Membr. Sci.* **2016**, *520*, 515−528.

(3) Surwade, S. P.; Smirnov, S. N.; Vlassiouk, I. V.; Unocic, R. R.; Veith, G. M.; Dai, S.; Mahurin, S. M. Water desalination using nanoporous single-layer graphene. *Nat. Nanotechnol.* **2015**, *10* (5), 459−64.

(4) Jiang, Z.; Stein, D. Charge regulation in nanopore ionic field-effect transistors. *Phys. Rev. E: Stat., Nonlin, Soft Matter Phys.* **2011**, *83* (3), 031203.

(5) Youn, Y.; Han, S. Investigation of field effects in a solid-state nanopore transistor. *Phys. Chem. Chem. Phys.* **2015**, *17* (41), 27806−11.

(6) Wang, M.; Kang, Q. Electrochemomechanical energy conversion efficiency in silica nanochannels. *Microfluid. Nanofluid.* **2010**, *9* (2−3), 181−190.

(7) Cheah, W.-K.; Sim, Y.-L.; Yeoh, F.-Y. Amine-functionalized mesoporous silica for urea adsorption. *Mater. Chem. Phys.* **2016**, *175*, 151−157.

(8) Joseph, G. G. I.; Hart, M. W.; Homola, A. M.; McKean, D. R.; Schein, L. B.; Smith, B. A.; Swanson, S. A., Electrophoretic display. US Patent US5745094A, 1999.

(9) Celebi, A. T.; Barisik, M.; Beskok, A. Electric field controlled transport of water in graphene nano-channels. *J. Chem. Phys.* **2017**, *147* (16), 164311.

(10) Celebi, A. T.; Barisik, M.; Beskok, A. Surface charge-dependent transport of water in graphene nano-channels. *Microfluid. Nanofluid.* **2018**, DOI: 10.1007/s10404-017-2027-z.

(11) Vo, T. Q.; Barisik, M.; Kim, B. Near-surface viscosity effects on capillary rise of water in nanotubes. *Phys. Rev. E: Stat., Nonlin, Soft Matter Phys.* **2015**, *92* (5), 053009.

(12) Lyklema, J. *Fundamentals of Interface and Colloid Science: Solid Liquid Interfaces*; Academic Press, 1995; Vol. *2*.

(13) Li, D. *Electrokinetics In Microfluidics*; Elsevier/Academic Press, 2004.

(14) Kim, S. I.; Kim, S. J. Analysis of the electroviscous effects on pressure-driven flow in nanochannels using effective ionic concentrations. *Microfluid. Nanofluid.* **2018**, DOI: 10.1007/s10404-017-2029-x.

(15) Jing, D.; Bhushan, B. Electroviscous effect on fluid drag in a microchannel with large zeta potential. *Beilstein J. Nanotechnol.* **2015**, *6*, 2207−16.

(16) Chang, C.-C.; Yang, R.-J.; Wang, M.; Miau, J.-J.; Lebiga, V. Liquid flow retardation in nanospaces due to electroviscosity: Electrical double layer overlap, hydrodynamic slippage, and ambient atmospheric CO2 dissolution. *Phys. Fluids* **2012**, *24* (7), 072001.

(17) Soong, C. Y.; Hwang, P. W.; Wang, J. C. Analysis of pressure-driven electrokinetic flows in hydrophobic microchannels with slip-dependent zeta potential. *Microfluid. Nanofluid.* **2010**, *9* (2−3), 211−223.

(18) Çetin, B.; Travis, B. E.; Li, D. Analysis of the electro-viscous effects on pressure-driven liquid flow in a two-section heterogeneous microchannel. *Electrochim. Acta* **2008**, *54* (2), 660−664.

(19) Jing, D.; Yi, S. Electroosmotic Flow in Tree-Like Branching Microchannel Network. *Fractals* **2019**, *27* (06), 1950095.

(20) Jing, D.; He, L.; Wang, X. Optimization analysis of fractal tree-like microchannel network for electroviscous flow to realize minimum hydraulic resistance. *Int. J. Heat Mass Transfer* **2018**, *125*, 749−755.

(21) Cheng, Z.; Ning, Z.; Zhang, W.; Ke, S. Theoretical investigation of electroviscous flows in hydrophilic slit nanopores: Effects of ion concentration and pore size. *Phys. Fluids* **2020**, *32* (2), 022005.

(22) Huang, K.-D.; Yang, R.-J. Electrokinetic behaviour of overlapped electric double layers in nanofluidic channels. *Nanotechnology* **2007**, *18* (11), 115701.

(23) Andrade, E. N. D. C. D. C. The effect of an electric field on the viscosity of liquids. II. *Proc. R. Soc. London Series A. Mathematical and Physical Sciences* **1951**, *204* (1079), 449−464.

(24) Hsu, W. L.; Daiguji, H.; Dunstan, D. E.; Davidson, M. R.; Harvie, D. J. Electrokinetics of the silica and aqueous electrolyte solution interface: Viscoelectric effects. *Adv. Colloid Interface Sci.* **2016**, *234*, 108−131.

(25) Hsu, W.-L.; Harvie, D. J. E.; Davidson, M. R.; Dunstan, D. E.; Hwang, J.; Daiguji, H. Viscoelectric Effects in Nanochannel Electrokinetics. *J. Phys. Chem. C* **2017**, *121* (37), 20517−20523.

(26) Sen, T.; Barisik, M. Size dependent surface charge properties of silica nano-channels: double layer overlap and inlet/outlet effects. *Phys. Chem. Chem. Phys.* **2018**, *20* (24), 16719−16728.

(27) Baldessari, F.; Santiago, J. G. Electrokinetics in nanochannels: part I. Electric double layer overlap and channel-to-well equilibrium. *J. Colloid Interface Sci.* **2008**, *325* (2), 526−38.

(28) Yan, Y.; Sheng, Q.; Wang, C.; Xue, J.; Chang, H.-C. Energy Conversion Efficiency of Nanofluidic Batteries: Hydrodynamic Slip and Access Resistance. *J. Phys. Chem. C* **2013**, *117* (16), 8050−8061.

(29) Chang, C.-C.; Yang, R.-J. Electrokinetic energy conversion in micrometer-length nanofluidic channels. *Microfluid. Nanofluid.* **2010**, *9* (2−3), 225−241.

(30) Chein, R.; Liao, C.; Chen, H. Electrokinetic energy conversion efficiency analysis using nanoscale finite-length surface-charged capillaries. *J. Power Sources* **2009**, *187* (2), 461−470.

(31) Zhang, Y.; He, Y.; Tsutsui, M.; Miao, X. S.; Taniguchi, M. Short channel effects on electrokinetic energy conversion in solid-state nanopores. *Sci. Rep.* **2017**, *7*, 46661.

(32) Vlassiouk, I.; Smirnov, S.; Siwy, Z. Ionic selectivity of single nanochannels. *Nano Lett.* **2008**, *8* (7), 1978−85.

(33) Jing, D.; Song, J.; Sui, Y. I. Hydraulic and Thermal Performances of Laminar Flow in Fractal Treelike Branching Microchannel Network with Wall Velocity Slip. *Fractals* **2020**, *28* (02), 2050022−454.

(34) Jing, D.; Song, S.; Pan, Y.; Wang, X. Size dependences of hydraulic resistance and heat transfer of fluid flow in elliptical microchannel heat sinks with boundary slip. *Int. J. Heat Mass Transfer* **2018**, *119*, 647−653.

(35) Ren, Y.; Stein, D. Slip-enhanced electrokinetic energy conversion in nanofluidic channels. *Nanotechnology* **2008**, *19* (19), 195707.

(36) Bandopadhyay, A.; Hossain, S. S.; Chakraborty, S. Ionic size dependent electroviscous effects in ion-selective nanopores. *Langmuir* **2014**, *30* (24), 7251−8.

(37) Jamaati, J.; Niazmand, H.; Renksizbulut, M. Pressure-driven electrokinetic slip-flow in planar microchannels. *Int. J. Therm. Sci.* **2010**, *49* (7), 1165−1174.

(38) Jing, D.; Pan, Y.; Wang, X. The non-monotonic overlapping EDL-induced electroviscous effect with surface charge-dependent slip and its size dependence. *Int. J. Heat Mass Transfer* **2017**, *113*, 32−39.
(39) Navier, C. L. M. H. Mémoire sur les lois du mouvement des fluides. *Mem. Acad. Sci. Inst.* **1823**, 389−416.
(40) Bocquet, L.; Barrat, J. L. Hydrodynamic boundary conditions and correlation functions of confined fluids. *Phys. Rev. Lett.* **1993**, *70* (18), 2726−2729.
(41) Bocquet, L.; Barrat, J. L. Hydrodynamic boundary conditions, correlation functions, and Kubo relations for confined fluids. *Phys. Rev. E: Stat. Phys., Plasmas, Fluids, Relat. Interdiscip. Top.* **1994**, *49* (4), 3079−3092.
(42) Barrat, J.-L.; Bocquet, L. Large Slip Effect at a Nonwetting Fluid-Solid Interface. *Phys. Rev. Lett.* **1999**, *82* (23), 4671−4674.
(43) Marry, V.; DufrÊChe, J. F.; Jardat, M.; Turq, P. Equilibrium and electrokinetic phenomena in charged porous media from microscopic and mesoscopic models: electro-osmosis in montmorillonite. *Mol. Phys.* **2003**, *101* (20), 3111−3119.
(44) Joly, L.; Ybert, C.; Trizac, E.; Bocquet, L. Hydrodynamics within the electric double layer on slipping surfaces. *Phys. Rev. Lett.* **2004**, *93* (25), 257805.
(45) Celebi, A. T.; Beskok, A. Molecular and Continuum Transport Perspectives on Electroosmotic Slip Flows. *J. Phys. Chem. C* **2018**, *122* (17), 9699−9709.
(46) Kalyoncu, G.; Barisik, M. Analytical solution of micro-/nanoscale convective liquid flows in tubes and slits. *Microfluid. Nanofluid.* **2017**, *21* (9), 147.
(47) Huang, D. M.; Sendner, C.; Horinek, D.; Netz, R. R.; Bocquet, L. Water slippage versus contact angle: a quasiuniversal relationship. *Phys. Rev. Lett.* **2008**, *101* (22), 226101.
(48) Sofos, F.; Karakasidis, T.; Liakopoulos, A. Parameters Affecting Slip Length at the Nanoscale. *J. Comput. Theor. Nanosci.* **2013**, *10* (3), 648−650.
(49) Zhang, C.; Chen, Y. Slip behavior of liquid flow in rough nanochannels. *Chem. Eng. Process.* **2014**, *85*, 203−208.
(50) Ramos-Alvarado, B.; Kumar, S.; Peterson, G. P. Hydrodynamic slip in silicon nanochannels. *Phys. Rev. E: Stat. Phys., Plasmas, Fluids, Relat. Interdiscip. Top.* **2016**, *93* (3), 033117.
(51) Yen, T.-H.; Soong, C.-Y. Effective boundary slip and wetting characteristics of water on substrates with effects of surface morphology. *Mol. Phys.* **2016**, *114* (6), 797−809.
(52) Barisik, M.; Beskok, A. Wetting characterisation of silicon (1,0,0) surface. *Mol. Simul.* **2013**, *39* (9), 700−709.
(53) Nguyen, C. T.; Barisik, M.; Kim, B. Wetting of chemically heterogeneous striped surfaces: Molecular dynamics simulations. *AIP Adv.* **2018**, *8* (6), 065003.
(54) Joly, L.; Ybert, C.; Trizac, E.; Bocquet, L. Liquid friction on charged surfaces: from hydrodynamic slippage to electrokinetics. *J. Chem. Phys.* **2006**, *125* (20), 204716.
(55) Malekidelarestaqi, M.; Mansouri, A.; Chini, S. F. Electrokinetic energy conversion in a finite length superhydrophobic microchannel. *Chem. Phys. Lett.* **2018**, *703*, 72−79.
(56) Rezaei, M.; Azimian, A. R.; Pishevar, A. R.; Bonthuis, D. J. Viscous interfacial layer formation causes electroosmotic mobility reversal in monovalent electrolytes. *Phys. Chem. Chem. Phys.* **2018**, *20* (35), 22517−22524.
(57) Celebi, A. T.; Cetin, B.; Beskok, A. Molecular and Continuum Perspectives on Intermediate and Flow Reversal Regimes in Electroosmotic Transport. *J. Phys. Chem. C* **2019**, *123* (22), 14024−14035.
(58) Jing, D.; Bhushan, B. Effect of boundary slip and surface charge on the pressure-driven flow. *J. Colloid Interface Sci.* **2013**, *392*, 15−26.
(59) Pan, Y.; Bhushan, B. Role of surface charge on boundary slip in fluid flow. *J. Colloid Interface Sci.* **2013**, *392*, 117−121.
(60) Barisik, M.; Atalay, S.; Beskok, A.; Qian, S. Size Dependent Surface Charge Properties of Silica Nanoparticles. *J. Phys. Chem. C* **2014**, *118* (4), 1836−1842.
(61) Atalay, S.; Barisik, M.; Beskok, A.; Qian, S. Surface Charge of a Nanoparticle Interacting with a Flat Substrate. *J. Phys. Chem. C* **2014**, *118* (20), 10927−10935.
(62) Ninham, B. W.; Parsegian, V. A. Electrostatic potential between surfaces bearing ionizable groups in ionic equilibrium with physiologic saline solution. *J. Theor. Biol.* **1971**, *31* (3), 405−428.
(63) Hoffmann, J.; Gillespie, D. Ion correlations in nanofluidic channels: effects of ion size, valence, and concentration on voltage- and pressure-driven currents. *Langmuir* **2013**, *29* (4), 1303−17.
(64) Hart, J. Correction to the Viscoelectric Constant. *J. Chem. Phys.* **1958**, *29* (4), 960−961.
(65) Lyklema, J.; Overbeek, J. T. G. On the interpretation of electrokinetic potentials. *J. Colloid Sci.* **1961**, *16* (5), 501−512.
(66) Hunter, R. J. The interpretation of electrokinetic potentials. *J. Colloid Interface Sci.* **1966**, *22* (3), 231−239.
(67) Stigter, D. On the Viscoelectric Effect in Colloidal Solutions. *J. Phys. Chem.* **1964**, *68* (12), 3600−3602.
(68) Freund, J. B. Electro-osmosis in a nanometer-scale channel studied by atomistic simulation. *J. Chem. Phys.* **2002**, *116* (5), 2194−2200.
(69) Qiao, R.; Aluru, N. R. Ion concentrations and velocity profiles in nanochannel electroosmotic flows. *J. Chem. Phys.* **2003**, *118* (10), 4692−4701.
(70) Qiao, R.; Aluru, N. R. Scaling of electrokinetic transport in nanometer channels. *Langmuir* **2005**, *21* (19), 8972−7.
(71) Hunter, R. J.; Leyendekkers, J. V. Viscoelectric coefficient for water. *J. Chem. Soc., Faraday Trans. 1* **1978**, *74* (0), 450−455.
(72) Bazant, M. Z.; Kilic, M. S.; Storey, B. D.; Ajdari, A. Towards an understanding of induced-charge electrokinetics at large applied voltages in concentrated solutions. *Adv. Colloid Interface Sci.* **2009**, *152* (1−2), 48−88.
(73) Bikerman, J. J. XXXIX. Structure and capacity of electrical double layer. *London, Edinburgh Dublin Philos. Mag. J. Sci.* **1942**, *33* (220), 384−397.
(74) Storey, B. D.; Bazant, M. Z. Effects of electrostatic correlations on electrokinetic phenomena. *Phys. Rev. E: Stat., Nonlin, Soft Matter Phys.* **2012**, *86* (5), 056303.
(75) Lyklema, J. On the slip process in electrokinetics. *Colloids Surf., A* **1994**, *92* (1−2), 41−49.
(76) Jing, D.; Bhushan, B. Quantification of surface charge density and its effect on boundary slip. *Langmuir* **2013**, *29* (23), 6953−63.
(77) Li, Y.; Bhushan, B. The effect of surface charge on the boundary slip of various oleophilic/phobic surfaces immersed in liquids. *Soft Matter* **2015**, *11* (38), 7680−95.
(78) Ghorbanian, J.; Celebi, A. T.; Beskok, A. A phenomenological continuum model for force-driven nano-channel liquid flows. *J. Chem. Phys.* **2016**, *145* (18), 184109.
(79) Hughes, C.; Yeh, L.-H.; Qian, S. Field Effect Modulation of Surface Charge Property and Electroosmotic Flow in a Nanochannel: Stern Layer Effect. *J. Phys. Chem. C* **2013**, *117* (18), 9322−9331.
(80) Trefalt, G.; Behrens, S. H.; Borkovec, M. Charge Regulation in the Electrical Double Layer: Ion Adsorption and Surface Interactions. *Langmuir* **2016**, *32* (2), 380−400.
(81) Sadeghi, M.; Saidi, M. H.; Sadeghi, A. Electroosmotic flow and ionic conductance in a pH-regulated rectangular nanochannel. *Phys. Fluids* **2017**, *29* (6), 062002.
(82) Nosrati, R.; Hadigol, M.; Raisee, M.; Nourbakhsh, A. Numerical Modeling of Electroosmotic Nanoflows with Overlapped Electric Double Layer. *J. Comput. Theor. Nanosci.* **2012**, *9* (12), 2228−2239.
(83) Sen, T.; Barisik, M. Internal surface electric charge characterization of mesoporous silica. *Sci. Rep.* **2019**, *9* (1), 137.
(84) Sen, T.; Barisik, M. Pore connectivity effects on the internal surface electric charge of mesoporous silica. *Colloid Polym. Sci.* **2019**, *297* (10), 1365−1373.
(85) Ozcelik, H. G.; Barisik, M. Electric charge of nanopatterned silica surfaces. *Phys. Chem. Chem. Phys.* **2019**, *21* (14), 7576−7587.

https://dx.doi.org/10.1021/acs.langmuir.0c01457
Langmuir 2020, 36, 9191−9203

(86) Ma, Y.; Yeh, L. H.; Lin, C. Y.; Mei, L.; Qian, S. pH-regulated ionic conductance in a nanochannel with overlapped electric double layers. *Anal. Chem.* **2015**, *87* (8), 4508−14.
(87) Andersen, M. B.; Frey, J.; Pennathur, S.; Bruus, H. Surface-dependent chemical equilibrium constants and capacitances for bare and 3-cyanopropyldimethylchlorosilane coated silica nanochannels. *J. Colloid Interface Sci.* **2011**, *353* (1), 301−10.
(88) Alan, B. O.; Barisik, M.; Ozcelik, H. G. Roughness Effects on the Surface Charge Properties of Silica Nanoparticles. *J. Phys. Chem. C* **2020**, *124* (13), 7274−7286.
(89) Yeh, L.-H.; Liu, K.-L.; Hsu, J.-P. Importance of Ionic Polarization Effect on the Electrophoretic Behavior of Polyelectrolyte Nanoparticles in Aqueous Electrolyte Solutions. *J. Phys. Chem. C* **2012**, *116* (1), 367−373.
(90) Mei, L.; Yeh, L.-H.; Qian, S. Buffer anions can enormously enhance the electrokinetic energy conversion in nanofluidics with highly overlapped double layers. *Nano Energy* **2017**, *32*, 374−381.
(91) Kalyoncu, G. Investigation of liquid transport in micro and nanoscale porous media at different pore to throat size ratios; Izmir Institute of Technology, 2017.
(92) Bazant, M. Z.; Sabri Kilic, M.; Storey, B. D.; Ajdari, A. Nonlinear electrokinetics at large voltages. *New J. Phys.* **2009**, *11* (7), 075016.

https://dx.doi.org/10.1021/acs.langmuir.0c01457
Langmuir 2020, 36, 9191−9203